



Development of a PARCS/Serpent model for neutronics analysis of the Dalat nuclear research reactor

Viet-Phu Tran¹ · Kien-Cuong Nguyen² · Donny Hartanto³ · Hoai-Nam Tran^{4,5} · Vinh Thanh Tran^{1,6} · Van-Khanh Hoang¹ · Pham Nhu Viet Ha¹

Received: 30 July 2020 / Revised: 30 November 2020 / Accepted: 2 December 2020 / Published online: 15 February 2021
© China Science Publishing & Media Ltd. (Science Press), Shanghai Institute of Applied Physics, the Chinese Academy of Sciences, Chinese Nuclear Society 2021

Abstract Cross-sectional homogenization for full-core calculations of small and complex reactor configurations, such as research reactors, has been recently recognized as an interesting and challenging topic. This paper presents the development of a PARCS/Serpent model for the neutronics analysis of a research reactor type TRIGA Mark-II loaded with Russian VVR-M2 fuel (known as the Dalat Nuclear Research Reactor or DNRR). The full-scale DNRR model and a supercell model for a shim/safety rod

and its surrounding fuel bundles with the Monte Carlo code Serpent 2 were proposed to generate homogenized few-group cross sections for full-core diffusion calculations with PARCS. The full-scale DNRR model with Serpent 2 was also utilized as a reference to verify the PARCS/Serpent calculations. Comparison of the effective neutron multiplication factors, radial and axial core power distributions, and control rod worths showed a generally good agreement between PARCS and Serpent 2. In addition, the discrepancies between the PARCS and Serpent 2 results are also discussed. Consequently, the results indicate the applicability of the PARCS/Serpent model for further steady state and transient analyses of the DNRR.

This study was funded by the Ministry of Science and Technology of Vietnam (No. DTCB.06/18/VKHKTHN).

✉ Kien-Cuong Nguyen
cuongnk.re@dnri.vn

✉ Pham Nhu Viet Ha
phamha@vinatom.gov.vn

¹ Institute for Nuclear Science and Technology (INST), Vietnam Atomic Energy Institute (VINATOM), 179 Hoang Quoc Viet str., Cau Giay District, Hanoi 100000, Vietnam

² Nuclear Research Institute (NRI), Vietnam Atomic Energy Institute (VINATOM), 01 Nguyen Tu Luc, Dalat, Lamdong 670000, Vietnam

³ Department of Mechanical and Nuclear Engineering, University of Sharjah, PO. BOX 27272, Sharjah, United Arab Emirates

⁴ Institute of Fundamental and Applied Sciences, Duy Tan University, Ho Chi Minh city 700000, Vietnam

⁵ Faculty of Natural Science, Duy Tan University, Danang 550000, Vietnam

⁶ Nuclear Safety Division, Technical Support Center for Radiation and Nuclear Safety and Emergency Response, Vietnam Agency for Radiation and Nuclear Safety (VARANS), 113 Tran Duy Hung str., Cau Giay District, Hanoi 100000, Vietnam

Keywords PARCS · Serpent 2 · Group constant · DNRR

1 Introduction

Deterministic and Monte Carlo (MC) lattice physics codes (e.g., [1–4]) have been widely used to generate homogenized multi-group cross sections for full-core calculations of power reactors, especially the deterministic ones. These multi-group constants are generally required for nodal diffusion codes to predict the behavior of a reactor core under steady-state and transient conditions. Recently, coupling modern calculation codes, e.g., Serpent [1], TRITON [2], HELIOS [3], and PARCS [5], which have been successfully applied to the modeling of large power reactors, particularly for few-group cross-sectional generation and 3D neutronics modeling of small research reactors [6–8] and generally for small reactor configurations [9] has been recognized as an interesting and challenging topic. For small and complicated reactor cores such

as research reactors, the use of continuous-energy MC codes (such as Serpent) appears to be a more appropriate choice for homogenized few-group cross-sectional generation than conventional deterministic codes [6, 10–14]. This is because the tight neutronics coupling of the components in research reactors may require full-scale reactor modeling for homogenized cross-sectional generation, and such requirements can be satisfied using MC lattice physics codes, such as Serpent. In addition, the use of MC methods can facilitate handling of the complex geometries of research reactors with the least approximation while allowing the utilization of continuous-energy neutron cross sections. However, there are existing challenges to the more accurate and efficient modeling and calculations of such small reactor configurations, such as correction of substantial neutron leakage for cross-sectional homogenization of the CROCUS [6] and VR-1 [7] research reactors, proper approximation of the thermal–hydraulic conditions for full-core diffusion calculations of the LVR-15 research reactor with PARCS [8], and elevated computational costs associated with MC methods [15, 16], especially for whole reactor modeling with fine and long burnup steps.

The aim of this study is to apply the PARCS and Serpent codes for neutronics analysis of the Dalat Nuclear Research Reactor (DNRR) [17] (a TRIGA Mark-II reactor [18] loaded with Russian VVR-M2 fuel) with a configuration significantly different and more complicated than those reported in previous studies, including the CROCUS [6], VR-1 [7], and LVR-15 [8] research reactors. The ultimate goal is to apply these two codes (namely PARCS and Serpent) to further transient and safety analyses of the DNRR and is aimed at updating the safety analysis report of the DNRR for the extension of its operation in the future. As the DNRR has a complex geometry with various components (such as fuel bundles, neutron trap, water gaps, irradiation channels, beryllium blocks, control rods, rotary specimen rack, graphite reflector, horizontal beam ports, thermal column, and thermalizing column), precise simulation of the DNRR is difficult, especially when using traditional deterministic codes. Therefore, MC codes, such as MCNP [19] and Serpent, appear to be the appropriate choice for simulating the complicated geometry of the DNRR. The MC code Serpent 2 was selected in this study for modeling of the DNRR owing to its flexible capability of generating homogenized few-group cross sections based on both the lattice and full-scale reactor configurations for nodal diffusion codes, such as PARCS. Moreover, the full-scale DNRR model with Serpent can be used as a reference to verify PARCS calculations that use the few-group cross sections generated by Serpent. The general methodologies for few-group cross-sectional homogenization of the DNRR with Serpent and full-core diffusion calculations of

the DNRR with PARCS were adopted herein similar to Refs. [6, 7]. Nevertheless, the full-scale DNRR modeled with Serpent covers the active core through the reactor tank to take advantage of the actual whole-core leakage spectrum for few-group cross-sectional homogenization and thereby, eliminates the need for neutron leakage correction, as reported for small reactor cores [6, 7]. Furthermore, to enable the full-core diffusion calculations of the DNRR with PARCS, a supercell model with Serpent was developed for cross-sectional homogenization of a shim or safety rod and its surrounding fuel bundles.

In this study, we propose and discuss a PARCS and Serpent coupled model (hereafter referred to as the PARCS/Serpent or PARCS model) for neutronics analysis of the DNRR loaded with low-enriched uranium (LEU) fuel. The full-scale model of the DNRR with Serpent 2 was used to generate the fuel and non-fuel few-group cross sections for the core and out-core regions, while a supercell model was used to generate the few-group cross sections for a shim or safety rod and its surrounding fuel bundles, for the PARCS calculations. The PARCS nodalization of the DNRR was based on the full-scale DNRR model with Serpent, with an equivalent configuration up to the graphite reflector. Subsequently, the effective neutron multiplication factor, radial and axial core power distributions, and control rod worths of the DNRR were determined with PARCS utilizing the few-group cross sections generated by Serpent. The full-scale DNRR model with Serpent was also used as a reference to verify the PARCS/Serpent calculations. The comparative results show a generally good agreement between PARCS/Serpent and Serpent, indicating the applicability of the developed PARCS/Serpent model for further steady-state and transient analyses of the DNRR.

2 Description and DNRR models

The 250 kW TRIGA Mark-II reactor, a pool-type multipurpose research reactor designed and manufactured by General Atomics, was installed in the Dalat Nuclear Research Institute (DNRI), Vietnam, in the early 1960s. The reactor was upgraded to 500 kW in the early 1980s and was named the DNRR. In this upgrade, the main structures of the TRIGA Mark-II reactor remained, while the reactor core was loaded with Russian VVR-M2 type HEU (highly enriched uranium with 36% ^{235}U enrichment) fuel bundles [20, 21] and cooled by natural convection. In accordance with the framework of the program on Russian Research Reactor Fuel Return (RRFR) and the program on the Reduced Enrichment for Research and Test Reactor (RERTR), the DNRR core was partially converted to LEU fuel with 19.75% ^{235}U enrichment in September 2007. The

full-core conversion to LEU fuel was performed during the period from November 24, 2011, to January 13, 2012 [17].

The horizontal and vertical cross-sectional views and the main specifications of the DNRR loaded with Russian VVR-M2 type LEU fuel bundles are shown in Fig. 1a, b, and Table 1, respectively. The reactor core consists of hexagonal

cells and includes fuel bundles, control rods, dry and wet irradiation channels, beryllium blocks, and a neutron trap (see Fig. 1c). The LEU fuel bundle is a VVR-M2 type composed of UO_2 -Al dispersion clad in aluminum, as displayed in Fig. 2a. The total ^{235}U mass in each LEU fuel bundle is ~ 49.7 g, distributed in three coaxial fuel tubes in which the

Fig. 1 (Color online)
Horizontal (a) and vertical (b) cross-sectional views of the DNRR (BT: horizontal beam port) and radial layout of the DNRR core configuration with 92 LEU fuel bundles (c) (SR: safety rod, ShR: shim rod, and AR: automatic regulating rod)

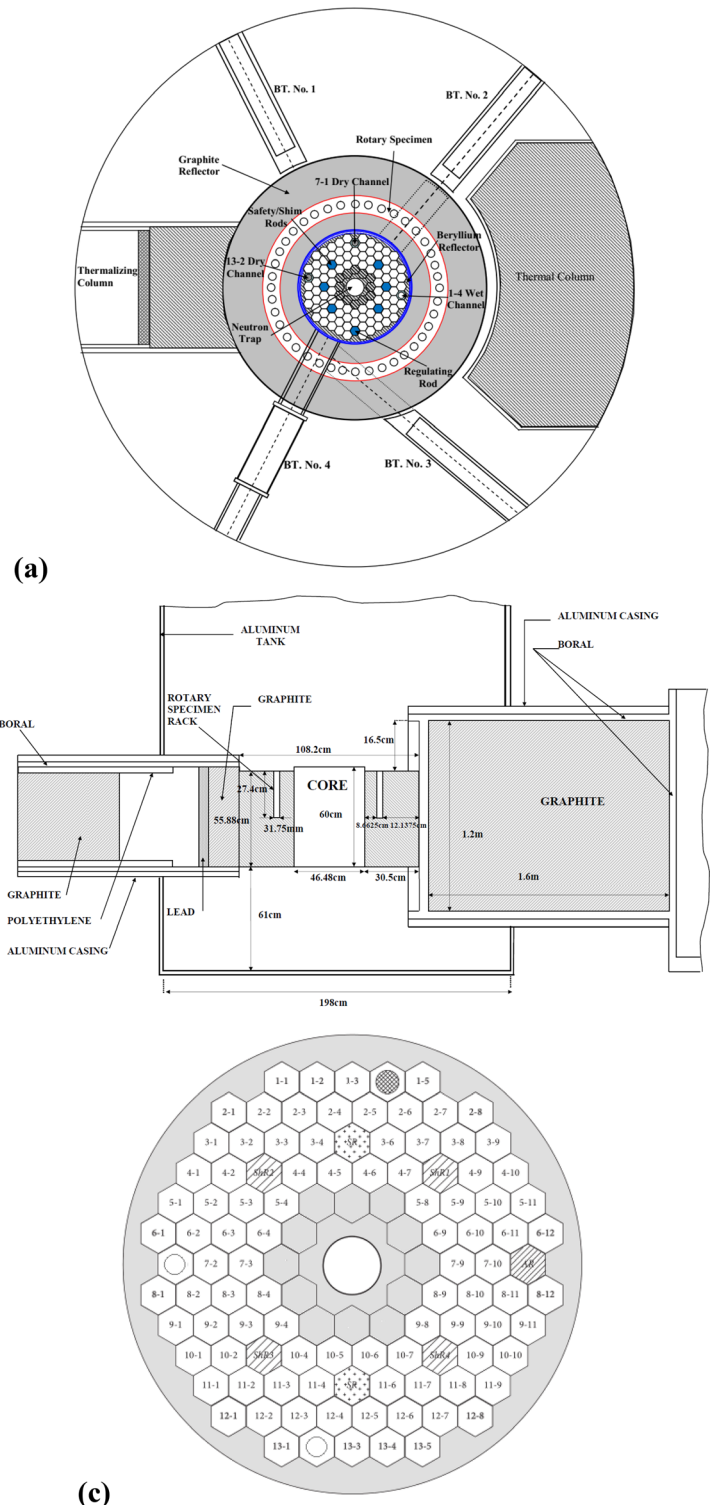


Table 1 Main specifications of the DNRR

Reactor type	Pool type
Nominal thermal power	500 kW
Coolant and moderator	Light water
Core cooling mechanism	Natural convection
Reflector	Graphite, beryllium, and light water
Active core height	60 cm
Core equivalent diameter	44.2 cm
Fuel pitch	3.5 cm
Fuel type	VVR-M2 type, dispersed UO ₂ -Al with 19.75% enrichment, aluminum cladding
Number of control rods	7 (2 safety rods, 4 shim rods, and 1 regulating rod)
Safety and shim rod material	B ₄ C
Automatic regulating rod material	Stainless steel
Vertical irradiation channels	4 (1 neutron trap, 1 wet channel, and 2 dry channels)
Horizontal beam ports	4 (1 tangential and 3 penetrant)

outer tube has a hexagonal shape, and the two inner tubes are cylindrical. The reactor control rod system consists of seven control rods, including two safety rods (composed of boron carbide), four shim rods (composed of boron carbide), and one automatic regulating rod (composed of stainless steel) (see Fig. 2b). Aluminum cylinders (with a thickness of 0.5 mm) cover the dry and wet channels, while the neutron trap (located at the core center) is a water cylinder that is 6.5 cm in diameter and 60 cm in length and is surrounded by the beryllium blocks, which have the same outer shape and dimensions as the fuel bundle. In addition, a ring of serrated beryllium blocks is located between the active core and graphite reflector to act as an additional reflector.

In this study, the DNRR loaded with the LEU fuel (see Fig. 1) was modeled using the MC code Serpent 2 for homogenized few-group cross-sectional generation and was nodalized using the nodal diffusion code PARCS for full-core diffusion calculations utilizing these few-group constants generated by Serpent. Using Serpent, the complex geometry of the DNRR, including the fuel bundles, control rods, in-core irradiation channels, beryllium blocks, horizontal beam ports, graphite reflector, rotary specimen rack, thermal column, and thermalizing column, was simulated with high accuracy. To simplify the simulation model without a significant impact on the neutronics characteristics of the DNRR core, the upper and lower parts of the fuel bundles, beryllium blocks, and dry and wet irradiation channels were described as homogeneous mixtures of aluminum and water. The calculation model with Serpent 2 covers the active core to the reactor tank in the radial direction with a diameter of 198.72 cm and in the axial direction with a height of 174.5 cm. The radial and axial layouts of the DNRR core modeled in Serpent 2 are illustrated in Fig. 3a and b. The DNRR model with PARCS

was simulated based on the full-scale DNRR model with Serpent with the same height and equivalent radial configuration up to the graphite reflector (see Fig. 4).

3 Codes and methods

PARCS, which was chosen by the U.S. Nuclear Regulatory Commission (NRC) as its best estimate core neutronics code, is a three-dimensional reactor core simulator that solves the steady-state and time-dependent multi-group neutron diffusion and low-order transport equations in orthogonal and non-orthogonal geometries [5]. PARCS can be used as a standalone code or coupled directly to the thermal hydraulics system code TRACE or RELAP5, which provides the temperature/flow field information to PARCS during transient calculations. PARCS uses the nodal cross sections generated by lattice physics codes, such as Serpent, TRITON, HELIOS, or CASMO [22]. In this investigation, the finite difference method (FDM) solver in PARCS code version v32m10co (distributed by the US NRC to the Regulator Body of Vietnam, Vietnam Agency for Radiation and Nuclear Safety, under the Code Assessment and Maintenance Program (CAMP) agreement) was selected for the DNRR full-core two-group diffusion calculations. The interface discontinuity factors and the multi-group diffusion option are not supported by the FDM solver in PARCS. Therefore, the spatial node sizes used for the PARCS nodalization of the DNRR with a hexagonal node size of 3.5 cm and hexagonal node height of 2.0 cm on average were chosen such that they were sufficiently small to achieve convergence in space [6, 7].

Serpent is a three-dimensional continuous-energy MC reactor physics burnup calculation code developed at the

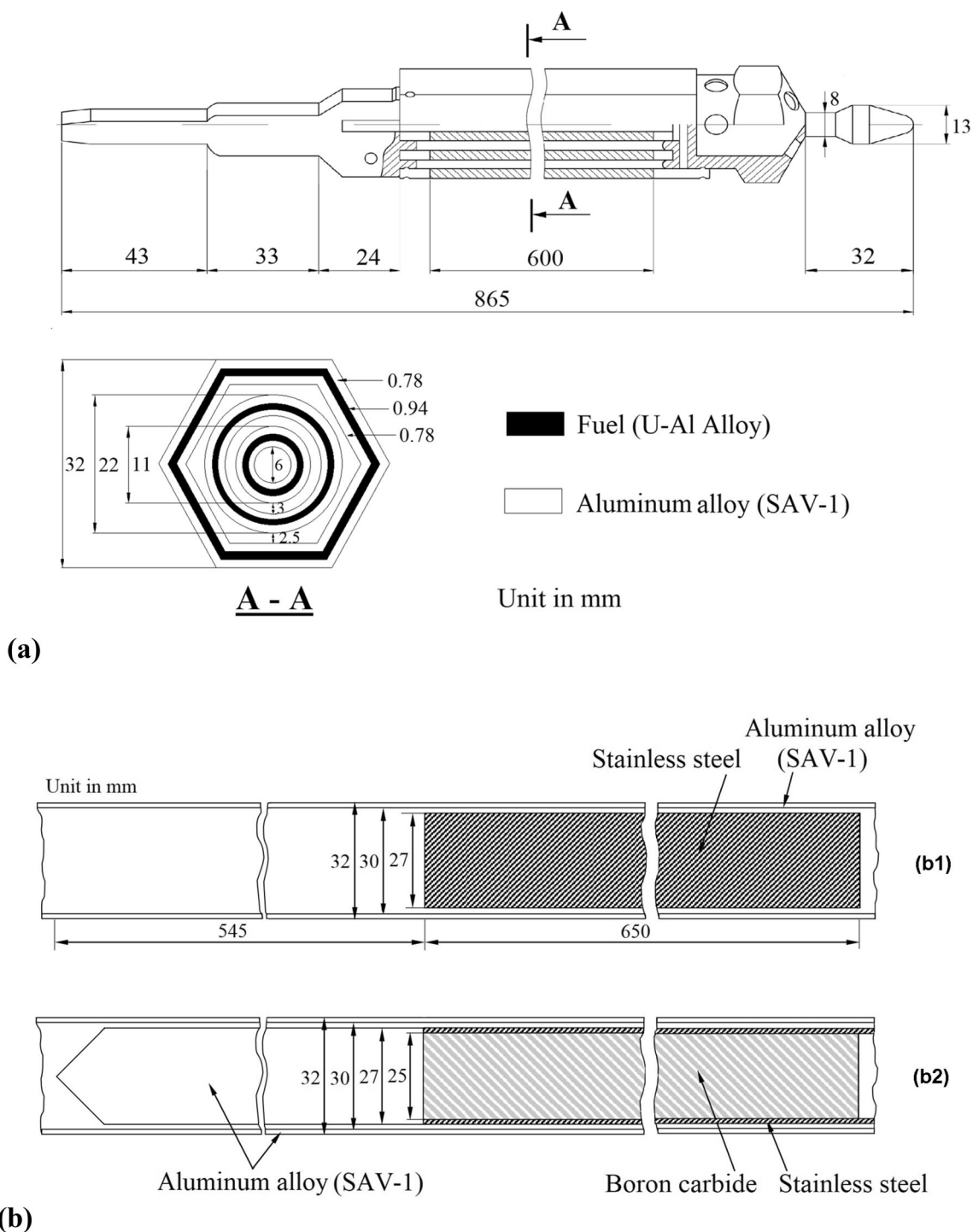


Fig. 2 The VVR-M2 type LEU fuel bundle (a) and vertical cross sections (b) of the (b1) automatic regulating rod and (b2) shim/safety rods in the DNRR

VTT Technical Research Centre of Finland [1]. The code allows the modeling of complicated reactor geometries for criticality calculations, fuel cycle studies, etc. Furthermore, it also has various powerful capabilities such as automated burnup sequence for spatial homogenization, coupled multi-physics calculations, transient simulations,

sensitivity calculations, reactor geometry pre-implementation, and fast running time. Serpent 2 has been widely used in calculations of nuclear reactors, in particular for TRIGA reactors [23, 24]. In this study, the full-scale DNRR model with Serpent 2 (Fig. 3a and b) was applied to generate homogenized few-group cross sections for full-core

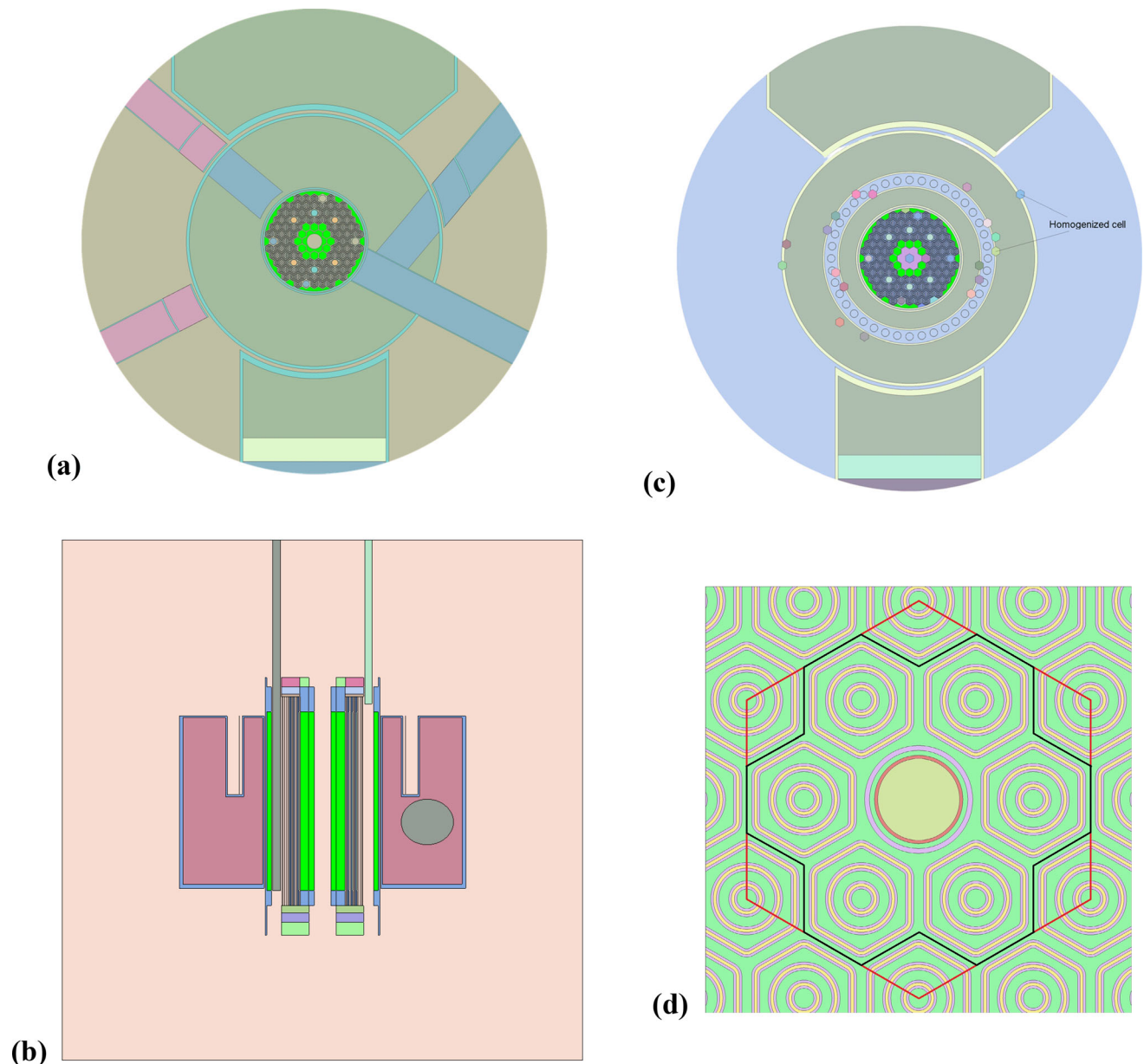


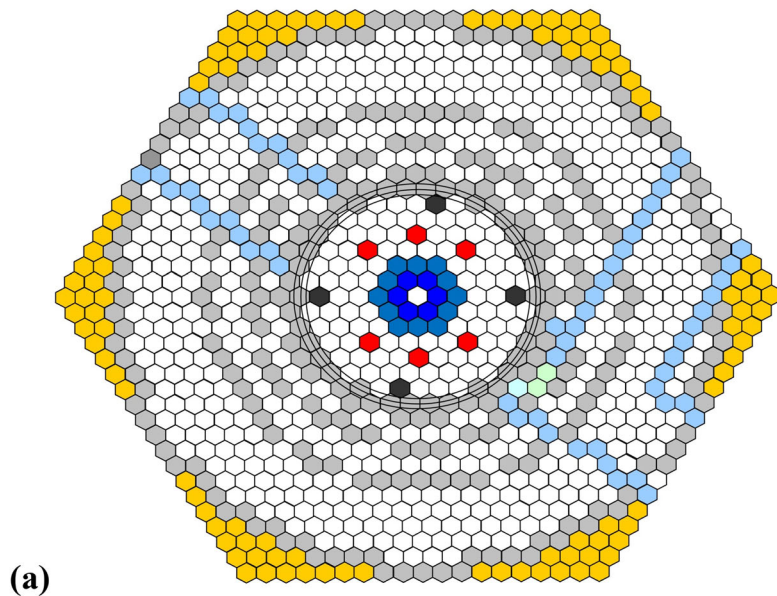
Fig. 3 (Color online) Radial (a) and axial (b) layouts of the full-scale DNRR modeled with Serpent. Radial layouts of the full-scale DNRR model with Serpent (c) and of the supercell model with Serpent (d) for homogenized few-group cross-sectional generation

diffusion calculations with PARCS and was also used to verify the PARCS/Serpent results. Using this model while noting that the DNRR uses graphite, beryllium, and light water as reflectors, the neutron leakage from the DNRR can be considered insignificant compared to those from the CROCUS [6] and VR-1 [7] research reactors. This could eliminate the need for neutron leakage correction, as reported for small reactor cores [6, 7] and allow the use of the out-scatter approximation for calculations of the diffusion coefficients for the DNRR. The ENDF/B-VII.1 nuclear data library [25] was used in the Serpent calculations. The energy cutoff was selected as 2.020 eV for two-

group cross-sectional generation. The WIMS 172 energy group structure [26] was used as the intermediate multi-group structure for the collapse of the two-group cross sections with Serpent [13]. We noted that the full-scale DNRR model with Serpent used in this study was verified against that with the MCNP5 Monte Carlo code [27], which has been extensively validated against experiments and other calculation results obtained with different codes [17, 28–30].

The full-scale DNRR model with Serpent was used to extract the fuel and non-fuel two-group cross sections, as illustrated in Fig. 3c. To account for the locations of the

Fig. 4 (Color online) Radial (a) and axial (b) layouts of the DNRR modeled with PARCS



Layer No.	Dimension (cm)	Reactor Core	Reflector
1	46.0	Water	Water
2	3.2	90wt% Water - 10wt% SAV1	Water
3	2.4	60wt% Water - 40wt% SAV1	Water
4	0.9	80wt% Water - 20wt% SAV1	Water
5	5.0	55.2wt% Water - 44.8wt% SAV1	Water
6	2.0	Fuel + Cladding + Water	Water
7	26.0	Fuel + Cladding + Water	Graphite Reflector Rotary Specimen Graphite Reflector
8	16.0	Fuel + Cladding + Water	Horizontal Beam Tube
9	14.0	Fuel + Cladding + Water	Graphite Reflector
10	2.0	Fuel + Cladding + Water	Water
11	5.0	55.2wt% Water - 44.8wt% SAV1	Water
12	2.4	80wt% Water - 20wt% SAV1	Water
13	3.3	85wt% Water - 15wt% SAV1	Water
14	4.3	90wt% Water - 10wt% SAV1	Water
15	42.0	Water	Water

(b)

fuel bundles, cross-sectional homogenization was performed for separate fuel bundles that were not adjacent to a shim or safety rod. Additionally, the non-fuel hexagonal nodes (homogenized cells) outside the DNRR core, as depicted in Fig. 4, were located at their equivalent positions in the full-scale DNRR model with Serpent for their two-group cross-sectional generation, along with the cross-sectional generation for the in-core regions. The purpose

was to take advantage of the actual full-core leakage spectrum for the homogenized two-group cross-sectional generation. Based on this approach, two-group cross-sectional data for 30 hexagonal nodes were generated to represent the out-core regions in the PARCS calculations. Similarly, two-group cross sections of the beryllium blocks, neutron trap, and other non-fuel regions in the core were also generated.

Homogenized few-group cross sections of the automatic regulating rod (composed of stainless steel) with the smallest worth as compared to those of the shim and safety rods (composed of B₄C) were also generated using the full-scale DNRR model with Serpent. To ensure an accurate solution from the FDM solver in PARCS when the highly absorbing material B₄C is present in the active core, the supercell model with Serpent (in which the absorption part of a shim or safety rod was homogenized with the surrounding fuel bundles) was used to generate the homogenized cross sections of the shim/safety rods and the neighboring fuel bundles when these control rods were inserted into the active core. The supercell model for a shim or safety rod and the surrounding fuel bundles was modeled as a radially infinite axially finite 3D geometry. The axial parts of the control rods and the surrounding fuel bundles, along with the water layers above and below the fuel bundles, were modeled as in the full-scale DNRR model. The radial layout of the supercell model is illustrated in Fig. 3d. In this model, six fuel bundles and a control rod were enclosed by a hexagonal boundary to enable the application of the reflective boundary condition in Serpent for the radial direction, and the vacuum boundary condition in the axial direction [31]. The supercells for the shim and safety rods can be embedded directly in the full-scale DNRR model with Serpent for their cross-sectional homogenization. However, this would require generating the cross-sectional sets of the supercells one by one when moving these control rods and would, therefore, be a time-consuming task. Using a separate supercell model, as previously mentioned, overcomes this disadvantage and takes advantage of the use of only one cross-sectional set generated for all of the shim and safety rods. This approximation can be considered reasonable and acceptable, taking into account the similar locations of these control rods in the DNRR core (Fig. 1a and c). The homogenized cross sections were then generated for the supercell, including a shim or safety rod and six fuel bundles. Similarly, homogenized cross sections of the aluminum followers (see Fig. 2b) of the shim/safety rods were also generated. Owing to such homogenization for use in the PARCS model, the power distributions of the fuel bundles surrounding the shim/safety rods must be reconstructed after the PARCS calculations. This power reconstruction was performed based on the reference power distributions calculated using Serpent, as explained below.

The power distribution ratio of each fuel bundle among the six bundles adjacent to a control rod, i.e., the form factor for the above-mentioned power reconstruction, was determined for the cases of inserted control rods simulated by PARCS as follows:

$$f'_{i,P} = f_{i,P} \times \frac{f'_{i,S}}{f_{i,S}}, \quad (1)$$

where f_i represents the power distribution ratio of each fuel bundle among the six bundles surrounding a control rod; $f_{i,S}$ and $f_{i,P}$ are the values of f_i in the all-rods-out case calculated by Serpent and PARCS, respectively; $f'_{i,S}$ is the value of f_i in the cases of inserted control rods calculated by Serpent; $f'_{i,P}$ is the form factor determined in the cases of inserted rods for the power reconstruction after the PARCS calculations.

The values of $f_{i,S}$, $f_{i,P}$, and $f'_{i,S}$ were calculated as follows:

$$f_i = \frac{P_i}{\sum_{k=1}^6 P_k}, \quad (2)$$

where P_i is the power distribution value of each fuel bundle adjacent to the control rod.

Each value of $f'_{i,P}$ was determined using Eq. (1), and normalized using Eq. (3):

$$f''_{i,P} = \frac{f'_{i,P}}{\sum_{j=1}^6 f'_{j,P}}. \quad (3)$$

The reconstructed power distribution for each fuel bundle among the six bundles surrounding a control rod was then determined for the cases of inserted rods simulated by PARCS as follows:

$$P''_{i,P} = f''_{i,P} \times \sum_{j=1}^7 P'_{j,P}, \quad (4)$$

where $P'_{j,P}$ ($j = 1, \dots, 7$) are the power distributions of the seven homogenized cells (resulting from the supercell model) calculated by PARCS in the cases of the inserted rods and $P''_{i,P}$ ($i = 1, \dots, 6$) are the reconstructed power distributions of the six fuel bundles adjacent to an inserted rod.

Finally, the full-scale DNRR model with Serpent was used as the reference to verify the PARCS/Serpent model for the DNRR under steady-state conditions. The parameters of the DNRR to be calculated and compared, including the effective neutron multiplication factor, radial and axial core power distributions, and control rod worths, are presented and discussed in the following section.

4 Results and discussion

4.1 Effective neutron multiplication factor

Table 2 lists the values of the effective multiplication factor (k_{eff}) obtained by Serpent and PARCS in the cases of (a) full insertion of the four shim rods and the automatic regulating rod in the core, (b) criticality condition (the

Table 2 Comparison of k_{eff} calculated using PARCS (P) and Serpent (S)

Case	Position of control rods (cm)		k_{eff}		
	Four shim rods	Regulating rod	Serpent	PARCS	P-S (pcm)
a	Full insertion	Full insertion	0.97355 ± 0.00007	0.96896	- 459
b	42	26	1.00083 ± 0.00007	0.99789	- 294
c	Complete withdrawal	Complete withdrawal	1.08118 ± 0.00007	1.08027	- 91
				1.08135*	17*

*The PARCS result in the case of using the cross sections of the aluminum followers for the control rods homogenized with the six surrounding fuel bundles generated using the supercell model

insertion of the four shim rods is 42 cm, and that of the regulating rod is 26 cm), and (c) complete withdrawal of the four shim rods and the regulating rod from the core. In all calculations, the two safety rods were assumed to be completely withdrawn from the core as they were used only for emergency shutdown. We also noted that the cross sections of the absorption parts of the four shim rods generated from the supercell model were used in Cases (a)–(b) when they were present in the active core; whereas the cross sections of the aluminum followers and the absorption parts of the two safety rods and the four shim rods generated by the full-scale DNRR model were used in Case (c) and Cases (a)–(b) when some of their absorption parts were located outside the active core.

There was generally good agreement among the k_{eff} values calculated using PARCS and Serpent. The PARCS results were also observed to underestimate the k_{eff} values predicted using the Serpent. An excellent agreement of - 91 pcm between PARCS and Serpent was found for Case (c) while their maximum disagreement of - 459 pcm was observed for Case (a), which is in line with those reported in Ref. [6] (- 418 pcm), Ref. [9] (- 526 pcm), and Ref. [7] (- 551 pcm) for small reactor cores. The trend in the difference between PARCS and Serpent, as listed in Table 2, can be explained by the presence of highly absorbing materials of the inserted shim rods in the active core for Cases (a)–(b), which renders the FDM solver of PARCS less accurate than when solving Case (c). Table 2 also indicates good agreement of 108 pcm in the k_{eff} value when using the following two different cross-sectional sets for the aluminum followers of the shim and safety rods in Case (c): (1) the cross cross sections of the aluminum followers of the control rods homogenized with the surrounding fuel bundles generated using the supercell model and (2) the cross sections of the aluminum followers and the surrounding fuel bundles generated separately using the full-scale DNRR model. In addition, the deviation of the radial power distributions when using these two different cross-sectional sets for the aluminum followers was confirmed to be as small as 0.6%. As this study aimed to verify the PARCS/Serpent model developed against the reference full-scale DNRR model at steady states, the cross sections

of the aluminum followers of the control rods generated using the full-scale DNRR model were used for verification purposes. However, the cross-sectional sets of the aluminum followers of the control rods homogenized with the surrounding fuel bundles generated using the supercell model should be used for transient calculations of the DNRR, as being planned in future studies.

4.2 Radial and axial core power distributions

In this section, the radial and axial core power distributions were calculated and analyzed using PARCS in comparison with the reference Serpent calculations. The two cases, including the core critical condition [Case (b)] and the complete withdrawal of the shim rods and regulating rod [Case (c)], as listed in Table 2, were considered. Figure 5a and b, which displays the radial power distributions calculated by Serpent and PARCS, shows good agreement between the two codes. The difference in the radial power distributions calculated by PARCS and Serpent was, however, as high as $\sim 10\%$, which appeared at the peripheral fuel bundles located adjacent to the beam ports No. 4 and 3 (see Fig. 1a). This discrepancy may be mainly attributed to the homogenization of the void region of beam port No. 4 and, to a lesser degree, that of beam port No. 3 in the core periphery with the adjacent graphite in the PARCS model, which leads to more neutron reflection back to the core and therefore, higher power density calculated by PARCS in this core periphery as compared to the Serpent results. Thus, treating such void regions in the PARCS/Serpent model to improve this discrepancy between PARCS and Serpent models should be carefully considered in future studies. In contrast, the difference in the radial power distributions calculated by PARCS and Serpent was as high as $\sim -8\%$ at the fuel bundles adjacent to the inner beryllium blocks. This can be explained by the effect of the homogenization of the neutron trap and the beryllium in the PARCS model, which results in less neutron reflection back to the adjacent fuel bundles and hence results in a lower power density as calculated by PARCS in this region in comparison with the Serpent values. Nonetheless, a difference within $\sim 10\%$ in

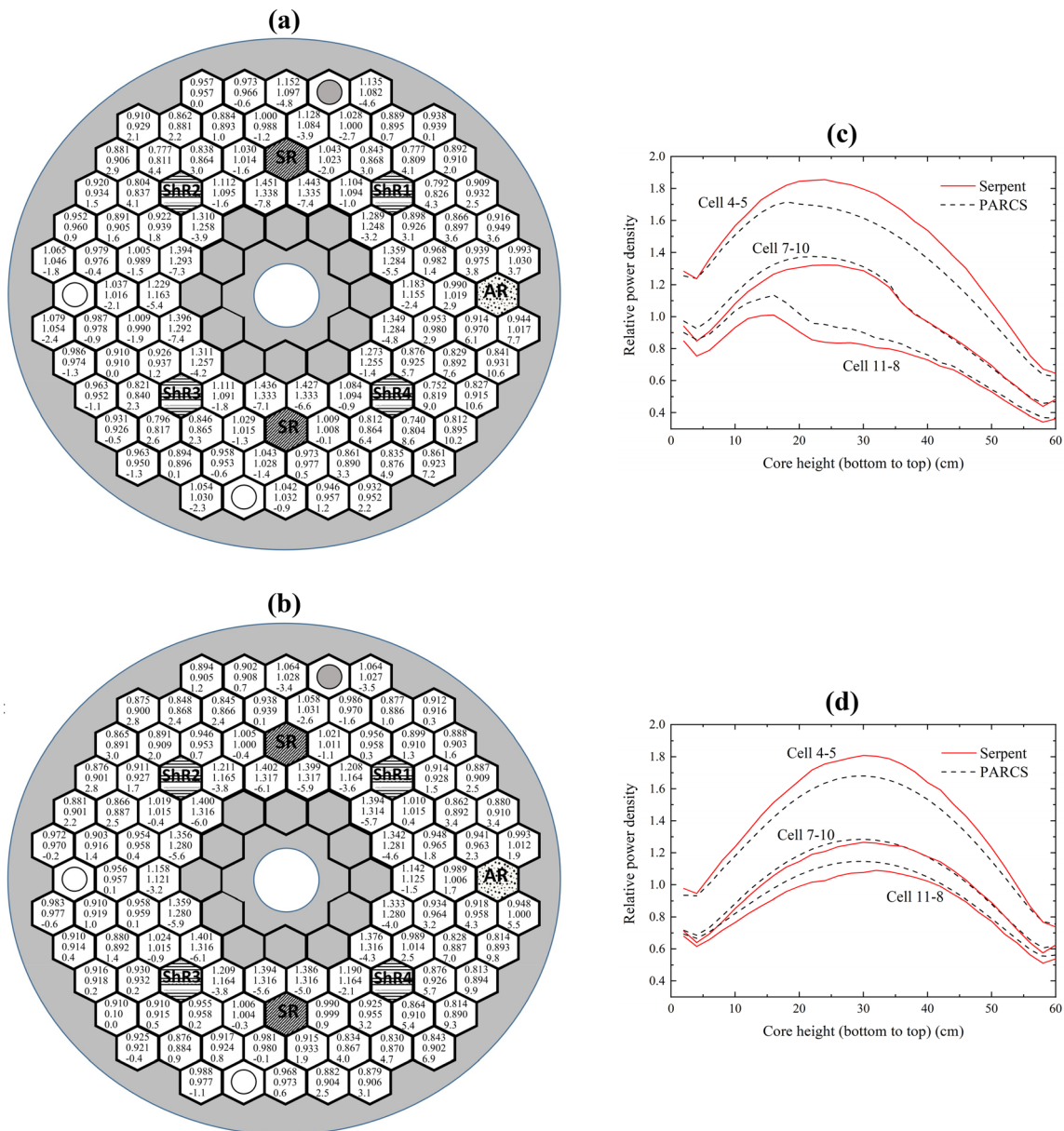


Fig. 5 (Color online) Comparison of the radial power distributions at the critical state (a), at the all-rods-out condition (b) upper cell value: Serpent; middle cell value: PARCS; lower cell value: relative percent

the radial power distributions (i.e., the radial thermal flux distributions) in the DNRR predicted by PARCS and Serpent was found to be comparable to the discrepancies reported within $\sim 15\%$ for the CROCUS [6] and VR-1 [7] research reactors.

The maxima of the relative power distributions calculated using PARCS and Serpent were found at cell 4–5 in both cases, indicating that the radial power profile calculated by PARCS agrees well with that predicted by Serpent. When the control rods were inserted in the core at the critical state [Case (b)], the relative power distributions of the fuel bundles adjacent to these control rods decreased

difference in PARCS and Serpent), and of the axial power distributions in cells 4–5, 7–10, and 11–8 at the critical state (c) and at the all-rods-out condition (d) calculated by PARCS and Serpent

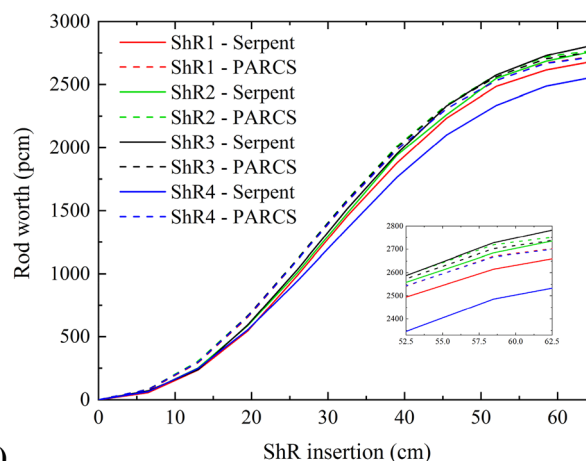
owing to the high neutron absorption of the inserted shim rods while those of the fuel bundles far from the inserted shim rods increased, as compared to the all-rods-out case [Case (c)]. Consequently, the radial power profile calculated by PARCS and Serpent in Case (b) became less flat than that in Case (c), and the disagreement between the PARCS and Serpent in predicting the radial power distributions in Case (b) increased, especially for the fuel bundles located near the inserted control rods.

The axial power distributions in cells 4–5, 7–10, and 11–8 (see Fig. 1c) calculated by PARCS and Serpent are shown in Fig. 5c and d. These cells were chosen for

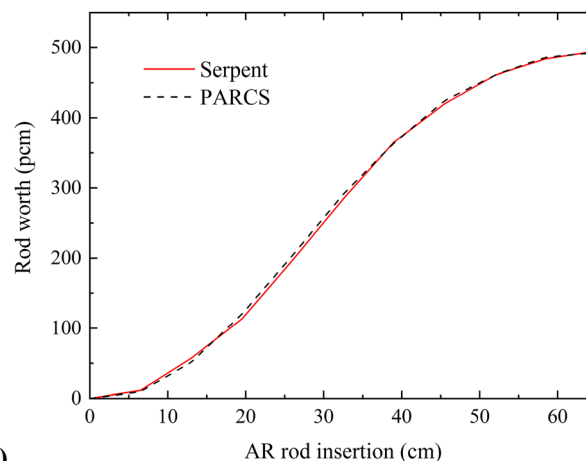
comparison of the axial power distributions obtained by the two codes because cell 4–5 is located near the inner beryllium blocks and has the highest relative radial power, while cells 7–10 and 11–8 are those next to the regulating rod and shim rod ShR4, respectively, which can clearly show the effects of control rod insertion and homogenization of the void regions of beam ports No. 3 and 4 adjacent to the core periphery with the nearby graphite in the PARCS model. Figure 5c and d exhibits an acceptable agreement of less than (1) ~ 12% for cell 4–5, (2) ~ 9% for cell 7–10, and (3) ~ 14% for cell 11–8 between the axial power distributions obtained with PARCS and Serpent. In addition, the difference in the axial power distributions in these cells obtained with PARCS and Serpent became more significant when the control rods were inserted in the core [Case (b)] as compared to the all-rods-out case [Case (c)]. The axial power distributions in cell 4–5 calculated by PARCS for both cases underestimated those predicted by Serpent, as explained above for the fuel bundles adjacent to the inner beryllium blocks. Meanwhile, the axial power distributions in cells 7–10 and 11–8 calculated by PARCS tended to overestimate those predicted by Serpent around the core midplane toward the core bottom. This may be due to the presence of beam ports No. 3 and 4 in this core axial region (see Fig. 4b) and consequently the effect of homogenization of the void regions of these beam ports near the core periphery with the adjacent graphite in the PARCS model, as discussed above.

4.3 Control rod worths

Control rod worth calculations were performed using PARCS and Serpent based on the initial critical reactor condition [Case (b) as listed in Table 2] from which each control rod was fully inserted into the core and then gradually withdrawn from the core to determine its worth. The worths of the shim, safety, and regulating rods calculated by PARCS and Serpent are listed in Table 3 and displayed in Fig. 6. Table 3 indicates that a good agreement within ~ 6% in the rod worths was obtained with PARCS and Serpent, which is consistent with the reported



(a)



(b)

Fig. 6 (Color online) Worths of the shim rods (a) and worth of the automatic regulating rod (b) calculated using PARCS and Serpent

discrepancy within ~ 8% for the VR-1 research reactor [7]. Additionally, Fig. 6a and b indicates that the worths of the shim and regulating rods calculated by PARCS generally overestimated those obtained by Serpent.

The worth of SR1 was also larger than that of SR2 in both the PARCS and Serpent calculations because of the fact that SR1 is located in the higher power density region, i.e., with higher thermal neutron fluxes, owing to the presence of the wet irradiation channel (see Fig. 5a). In a

Table 3 Comparison of the control rod worths calculated using PARCS (P) and Serpent (S)

Control rod	Serpent (pcm)	PARCS (pcm)	P-S (pcm)	Difference (%)
AR	495	493	- 2	- 0.4
ShR1	2,687	2,722	35	1.3
ShR2	2,767	2,771	4	0.2
ShR3	2,817	2,760	- 57	- 2.0
ShR4	2,562	2,720	158	6.1
SR1	2,311	2,173	- 138	- 6.0
SR2	2,218	2,140	- 78	- 3.5

similar manner, the worth of ShR4 is smallest among the four shim rods, as it is located in the lower power density region which is mainly caused by the presence of beam ports No. 3 and 4 adjacent to the core boundary. In particular, the worth of ShR4 calculated by PARCS overestimated that calculated by Serpent by $\sim 6\%$ because of the higher power density in this region predicted by PARCS when compared to Serpent, as discussed in Sect. 4.2. The agreement between PARCS and Serpent in predicting the control rod worths was also closely related to their agreement in the power distribution prediction, as shown in Fig. 5a.

5 Conclusion

This paper proposed a PARCS/Serpent model for neutronics analysis of the DNRR with a hexagonal configuration significantly different and more complicated than the CROCUS, VR-1, and LVR-15 research reactors with rectangular geometries. Homogenized two-group cross sections were generated using the full-scale DNRR model with Serpent 2 and used for the full-core diffusion calculations with PARCS. Using the full-scale DNRR model, the need for neutron leakage correction for the DNRR could be eliminated and the whole-core leakage spectrum could be utilized for cross-sectional homogenization, taking into account the tight neutronics coupling of the components in the DNRR. In addition, the supercell model with Serpent for cross-sectional homogenization of a shim or safety rod and its neighboring fuel bundles allows the utilization of the FDM solver of PARCS for full-core diffusion calculations of the DNRR. In addition, the full-scale DNRR model with Serpent can be used as a reference for verification of the PARCS/Serpent results is also an advantage. A comparison of the keff, radial and axial core power distributions, and control rod worths calculated by PARCS and Serpent showed a generally good agreement between the two codes, indicating the applicability of the PARCS/Serpent model developed for further steady-state and transient analyses of the DNRR.

The differences in the keff, core power distributions, and control rod worths obtained by PARCS and Serpent were also consistent with those reported for other small reactor cores, including the CROCUS [6], VR-1 [7], and LVR-15 [8] research reactors. However, the PARCS results for the DNRR were attributed to the inherent drawbacks of diffusion theory in the presence of highly absorbing materials or void regions and proximity to the core/reflector boundaries. The discrepancy in the radial power distributions obtained by PARCS and Serpent was found to be less than 5% for most of the fuel bundles, except at some core/reflector boundaries where it was as high as (1)

approximately -8% at the fuel bundles adjacent to the inner beryllium blocks and (2) $\sim 10\%$ at the core peripheral locations near beam port No. 4. The largest deviation in the axial power distributions was found to be as high as 14% for the analyzed cells located in close proximity to those core/reflector boundaries. Thus, we strongly suggest that special treatments for the reflector cross sections in those regions of the DNRR, e.g., by considering the transport cross-sectional optimization solution proposed in Ref. [32] for a diffusion solver or applying a radial reflector discontinuity factor iteration scheme recently proposed for VR-1 [33], should be closely examined in future studies.

The cross-sectional homogenization approach, based on the full-scale DNRR model with Serpent and the developed supercell model, has the flexibility of analyzing the full range of operating states of the DNRR owing to the automated burnup sequence for cross-sectional homogenization in Serpent. Although the full-scale DNRR calculations with Serpent for cross-sectional homogenization, especially for branch or history variations, are slightly computationally expensive owing to the nature of the MC method, they can be easily offset by rapid full-core calculations with PARCS. Another advantage of the PARCS/Serpent model for DNRR is that it can be directly coupled with the U.S. NRC thermal hydraulics system code TRACE or RELAP5 for 3D coupled neutron kinetics/thermal hydraulics calculations of the DNRR. Future studies will further improve the PARCS/Serpent model for DNRR to reduce the discrepancies between PARCS and Serpent, as well as to validate them against experimental data during reactor startup, thereafter apply them to transient and safety analyses of the DNRR.

Author contributions All authors contributed to the study conception and design. Material preparation, data collection, model development and analysis were performed by Viet-Phu Tran, Kien-Cuong Nguyen and Pham Nhu Viet Ha. The first draft of the manuscript was written by Pham Nhu Viet Ha and all authors commented on previous versions of the manuscript. All authors read and approved the final manuscript.

References

1. J. Leppänen, M. Pusa, T. Viitanen et al., The serpent monte carlo code: status, development and applications in 2013. *Ann. Nucl. Energy* **82**, 142–150 (2015). <https://doi.org/10.1016/j.anucene.2014.08.024>
2. R.S.I.C. Center, *A Comprehensive Modeling and Simulation Suite for Nuclear Safety Analysis and Design* (Oak Ridge, Tennessee, 2011).
3. R.J. Stammler, *Helios Methods* (Studsvik Scandpower, Sweden, 2009).
4. X. Qin, M. Li, H. Liao et al., Neutronics analysis of commercial pressurized water reactor loaded with FCM fuel. *Nuclear*

- Techniques **43**(8), 080007 (2020). <https://doi.org/10.11889/j.0253-3219.2020.hjs.43.080007> (in Chinese)
5. T. Downar, Y. Xu, V. Seker, PARCS v3.0 US NRC Core Neutronics Simulator - Theory Manual. RES/U.S. NRC, Rockville, Md (2012)
 6. A. Rais, D. Siefman, M. Hursin et al., Neutronics modeling of the CROCUS reactor with SERPENT and PARCS codes, in Proc. M&C 2017, Jeju, Korea, April 16–20 (2017)
 7. F. Fejt, J. Frybort, Analysis of a small-scale reactor core with PARCS/Serpent. Ann. Nucl. Energy **117**, 25–31 (2018). <https://doi.org/10.1016/j.anucene.2018.03.002>
 8. A. Dambrosio, M. Ruščák, G. Mazzini et al., Neutronic analysis of the LVR-15 research reactor using the PARCS code. Ann. Nucl. Energy **117**, 145–154 (2018). <https://doi.org/10.1016/j.anucene.2018.03.009>
 9. G. Baiocco, A. Petrucci, S. Bznuni et al., Analysis of a small PWR core with the PARCS/Helios and PARCS/Serpent code systems. Ann. Nucl. Energy **107**, 42–48 (2018). <https://doi.org/10.1016/j.anucene.2017.04.008>
 10. A. Rais, D. Siefman, G. Girardin et al., PARCS few-group homogenized parameters generation using Serpent Monte Carlo code at the CROCUS reactor. Proc. IGORR **2014**, 1–11 (2014)
 11. A. Rais, D. Siefman, G. Girardin et al., *Methods and Models for the Coupled Neutronics and Thermal-Hydraulics Analysis of the CROCUS Reactor at EFPL* (Technol. Nucl. Ins. Sci, 2015). <https://doi.org/10.1155/2015/237646>
 12. D. Siefman, G. Girardin, A. Rais et al., Full core modeling techniques for research reactors with irregular geometries using Serpent and PARCS applied to the CROCUS reactor. Ann. Nucl. Energy **85**, 434–443 (2015). <https://doi.org/10.1016/j.anucene.2015.05.004>
 13. J. Leppänen, M. Pusa, E. Fridman, Overview of methodology for spatial homogenization in the Serpent 2 Monte Carlo code. Ann. Nucl. Energy **96**, 126–136 (2016). <https://doi.org/10.1016/j.anucene.2016.06.007>
 14. G. Zhang, J. Liu, W.S. Yang, Application of PROTEUS-MOC for the steady state simulations of TREAT. Nucl. Tech. **43**(4), 040008 (2020). <https://doi.org/10.11889/j.0253-3219.2020.hjs.43.040008> (in Chinese)
 15. S.B. Alam, D. Kumar, B. Almutairi et al., Lattice benchmarking of deterministic, Monte Carlo and hybrid Monte Carlo reactor physics codes for the soluble-boron-free SMR cores. Nucl. Eng. Des. **356**, 110350 (2020). <https://doi.org/10.1016/j.nucengdes.2019.110350>
 16. T. Li, K. Zhuang, W. Shang et al., Preliminary neutronics design of space nuclear reactor based on molten salt cooling. Nucl. Tech. **43**(8), 080006 (2020). <https://doi.org/10.11889/j.0253-3219.2020.hjs.43.080006> (in Chinese)
 17. NRI, Safety analysis report for the Dalat nuclear research reactor. Nuclear Research Institute, Dalat, Viet Nam (2012)
 18. IAEA, History, Development, and Future of TRIGA Research Reactors. Technical Reports Series No. 482 (2016).
 19. D.B. (editor) Pelowitz, MCNP6TM User's Manual, Version 1.0. LA-CP-13-00634, Rev. 0, Los Alamos National Laboratory, May (2013).
 20. Q.B. Do, H.N. Tran, Q.H. Ngo et al., Determination of fuel burnup distribution of a research reactor based on measurements at subcritical conditions. Nucl. Sci. Tech. **29**, 174 (2018). <https://doi.org/10.1007/s41365-018-0511-0>
 21. G.T.T. Phan, Q.B. Do, Q.H. Ngo et al., Application of differential evolution algorithm for fuel loading optimization of the DNRR research reactor. Nucl. Eng. Des. **362**, 110582 (2020). <https://doi.org/10.1016/j.nucengdes.2020.110582>
 22. J. Rhodes, K. Smith, D. Lee, Casmo-5 development and applications, in Proc. PHYSOR-2006, ANS Topical Meeting on Reactor Physics (2006).
 23. D. Čalić, G. Žerovnik, A. Trkov et al., Validation of the Serpent 2 code on TRIGA Mark II benchmark experiments. Appl. Radiat. Isot. **107**, 165–170 (2016). <https://doi.org/10.1016/j.apradiso.2015.10.022>
 24. C. Castagna, D. Chiesa, A. Cammi et al., A new model with Serpent for the first criticality benchmarks of the TRIGA Mark II reactor. Ann. Nucl. Energy **113**, 171–176 (2018). <https://doi.org/10.1016/j.anucene.2017.11.011>
 25. M.B. Chadwick, M. Herman, P. Obložinský, et al., ENDF/B-VII.1 nuclear data for science and technology: Cross sections, covariances, fission product yields and decay data. Nucl. Data Sheets **112** (12), 2887–2996 (2011). <https://doi.org/https://doi.org/10.1016/j.nds.2011.11.002>
 26. J. Leppänen, WIMS 172-group structure. Serpent Wiki (2020). http://serpent.vtt.fi/mediawiki/index.php/WIMS_172-group_structure. Accessed: 2020-06-20
 27. N.K. Cuong, N.T. Dung, T.V. Phu et al., Modeling of the Dalat nuclear research reactor (DNRR) with the Serpent 2 Monte Carlo code. Nucl. Sci. Technol. **9**(3), 21–29 (2019)
 28. L.B. Vien, L.V. Vinh, H.T. Nghiem et al., Design analyses for full core conversion of the Dalat nuclear research reactor. Nucl. Sci. Technol. **4**(1), 10–25 (2014)
 29. G. Phan, H.N. Tran, K.C. Nguyen et al., Comparative analysis of the Dalat nuclear research reactor with HEU fuel using SRAC and MCNP5. Sci. Technol. Nucl. Ins. **2017**, 2615409 (2017). <https://doi.org/10.1155/2017/2615409>
 30. Q.B. Do, G.T.T. Phan, K.C. Nguyen et al., Criticality and rod worth analysis of the DNRR research reactor using the SRAC and MCNP5 codes. Nucl. Eng. Des. **343**, 197–209 (2019). <https://doi.org/10.1016/j.nucengdes.2019.01.011>
 31. J. Leppänen, Boundary conditions. Serpent Wiki (2020). http://serpent.vtt.fi/mediawiki/index.php/Boundary_conditions. Accessed: 2020-10-20
 32. T. Clerc, A. Hbert, H. Leroyer et al., An advanced computational scheme for the optimization of 2D radial reflector calculations in pressurized water reactors. Nucl. Eng. Des. **273**, 560–575 (2014). <https://doi.org/10.1016/j.nucengdes.2014.03.044>
 33. P. Suk, Radial reflector discontinuity factors iteration scheme at VR1. Nucl. Eng. Des. **366**, 110737 (2020)